Title

The development of solid-state NMR of membrane proteins.

Journal

Biomedical Spectroscopy and Imaging, 3(2)

ISSN

2212-8794

Author

Opella, Stanley J

Publication Date

2014

DOI

10.3233/bsi-140080

Peer reviewed

HHS Public Access

Author manuscript

Biomed Spectrosc Imaging. Author manuscript; available in PMC 2015 June 09.

Published in final edited form as:

Biomed Spectrosc Imaging. 2014 ; 3(2): 81–105. doi:10.3233/BSI-140080.

The development of solid-state NMR of membrane proteins

Stanley J. Opella*

Department of Chemistry and Biochemistry, University of California, San Diego, La Jolla, California, USA

Abstract

Most biological functions are carried out in supramolecular assemblies. As a result of their slow reorientation in solution, these assemblies have been resistant to the widely employed solution NMR approaches. The development of solid-state NMR to first of all overcome the correlation time problem and then obtain informative high-resolution spectra of proteins in supramolecular assemblies, such as virus particles and membranes, is described here. High resolution solid-state NMR is deeply intertwined with the history of NMR, and the seminal paper was published in 1948. Although the general principles were understood by the end of the 1950s, it has taken more than fifty years for instrumentation and experimental methods to become equal to the technical problems presented by the biological assemblies of greatest interest. It is now possible to obtain atomic resolution structures of viral coat proteins in virus particles and membrane proteins in phospholipid bilayers by oriented sample solid-state NMR methods. The development of this aspect of the field of solid-state NMR is summarized in this review article.

Keywords

Membrane proteins; NMR spectroscopy; dipolar couplings; chemical shift anisotropy; protein structure determination; oriented sample solid-state NMR; magic angle spinning solid-state NMR; rotationally aligned solid-state NMR; GPCR; MerF; p7; phospholipid bilayers

1. Introduction

The Achilles' Heel of NMR spectroscopy, the correlation time problem, held back applications of NMR to membrane proteins in phospholipid bilayers for many years. However, high-resolution solid-state NMR is now sufficiently advanced to enable detailed studies, including structure determination, to be performed with the proteins under near-native conditions in phospholipid bilayers under physiological conditions. As is well known, the term "solid-state" NMR is a misnomer, since it refers to the instrumentation, experimental methods, and theory, but not the physical state of the sample. Solid-state NMR is applicable to molecules that reorient slowly compared to the relevant time scale, generally ~10^{-4} sec, dictated by the dipole-dipole and chemical shift interactions. The time scale can be shifted to significantly shorter times by observing spectra from quadrupolar nuclei, such as ^{2}H and ^{14}N. Biological supramolecular assemblies, such as virus particles and

*Address for correspondence: Department of Chemistry and Biochemistry, University of California, San Diego, 9500 Gilman Drive 307,La Jolla, California, 92093-0307 USA., sopella@ucsd.edu.

membranes, reside in aqueous solution, but with their overall reorientation restricted by their mass and shape. Molecules and atomic sites that reorient fast undergo motional averaging, and if it is effectively isotropic, then solution NMR is the appropriate approach. Even though it is possible to determine the structures of membrane-associated polypeptides in micelles and bicelles by solution NMR, there is a significant hazard that the detergents present in the sample will distort the protein structures.

Membrane proteins are a prime example of structural biology where the advantages of determining the three dimensional structures of these proteins in phospholipid bilayers under physiological conditions are so overwhelming that it is likely that solid-state NMR will become the ‘gold standard’ for their characterization in the near future. Since membrane proteins constitute about one-third of the proteins expressed from a genome and include the major classes of drug receptors, this is highly significant.

2. Personal perspective

My graduate research was on solution NMR of proteins, primarily the implementation of natural abundance ^{13}C NMR [66] using one of the first commercial spectrometers equipped with an accessory for pulsed Fourier Transform operation. Tellingly, one of the experiments was the characterization of the rotational correlation time of a globular protein by relaxation measurements of the backbone $^{13}C\alpha$ sites [4]. The NMR’s ‘size problem’ of common parlance is more accurately the ‘correlation time problem’, and it has been paramount in all solution NMR studies of proteins, starting with the initial spectrum [94], and continuing through the present [12], despite the enormous strides that have been made in sample preparation, experimental methods, and instrumentation.

During my graduate research, even before the advent of heterologous expression of almost any protein from a genome, there was a continuous stream of new proteins potentially available for study by NMR spectroscopy. But one question was asked in every conversation about a new protein: how big is it? And equally important was consideration of the protein’s solubility and tendency towards aggregation. Central to the correlation time problem is the overall organization of biological systems, with most biological functions carried out within supramolecular complexes, such as membranes, virus particles, chromatin, etc. The correlation time problem was feared since if the questions were answered unsatisfactorily, and they usually were, the conversation would stop.

After my graduate research I wanted to address the ‘show stopping’ issue of the correlation time problem. For a time, it seemed that I would have to learn an entirely new technique, such as crystallography or optical spectroscopy, even though both are limited compared to NMR’s atomic resolution details about protein structure, dynamics, and interactions. The answer as to what to do for postdoctoral research was contained in the paper “Proton-Enhanced Nuclear Induction Spectroscopy. A Method for High-Resolution NMR of Dilute Spins in Solids” by Pines, Gibby, and Waugh [86]. In this communication, they said: “One can thus contemplate high resolution NMR of very rare spins and/or very small samples. Studies of chemical shift anisotropy of rare species (e.g., metals bound to proteins) or the dipolar structure of rare spin groups (e.g., ^{31}P of polyphosphate moieties) could be of value

in structural studies." Taking their statement at face value, I convinced myself that with the use of isotopic labeling and the promised further development of the methods they could be applied to proteins in supramolecular assemblies. I was fortunate to be able to pursue postdoctoral research in John Waugh's laboratory at M.I.T. where high resolution solid-state NMR was invented [86, 111] and first applied to chemical [85] and biochemical [108] problems. My contribution was to help identify and develop those aspects that would enable it to be applied to proteins and other biological systems [67, 68]. The eighteen-month immersion in solid-state NMR that I obtained in the Waugh laboratory set the stage for establishing my own research group as an Assistant Professor.

The goal of my own research was simple, but ambitious. It was to develop and apply a general method for structure determination of proteins in biological supramolecular assemblies. The first example was filamentous bacteriophages [105], and as the approach has advanced it is now possible to determine the structures of membrane proteins in phospholipid bilayers [82]. Throughout, single- and poly-crystalline compounds were used as model systems for the development of new pulse sequences and instrumentation. This article describes my view of the development of solid-state NMR of proteins from the perspective of my own research program. Key influences are emphasized, but it is in no way meant to be a complete review of the field, and necessarily there are only a limited number of references to important complementary studies from other investigators. Recently, Ian Campbell wrote a similar review in this series [12], and hopefully others will in the future, in order to provide a full account of the development of biological NMR from multiple perspectives.

3. Historical perspective

3.1 Origins of NMR spectroscopy

In 1946 Bloch and Purcell defined the field of NMR spectroscopy [8, 89] by demonstrating that signals could be detected through the phenomenon of resonance. These groups worked out many aspects of nuclear magnetism and relaxation during the next few years. However, it is a paper by Pake in 1948 [74] that had a particular impact on the application of NMR to chemical problems, including structure determination and intramolecular dynamics [33–35, 75]. The original Pake paper [74] demonstrated the presence of the dipole-dipole nuclear spin interaction between two spin I=1/2 nuclei in close proximity. Because of the limitations of the instrumentation and experimental techniques available at the time, the success of the study rested on the choice of sample, since water molecules, with their proximate pair of hydrogens, on gypsum were well separated from each other, eliminating the necessity of homonuclear decoupling to observe the coupling between the isolated pair of ^{1}H in the water molecules. It was possible to prepare single crystal and powder samples for comparisons.

The original goal was to show that line widths obtained from solids were fundamentally broad. By inference, this would demonstrate that the line widths in liquids were narrow. The first surprise of NMR spectroscopy was finding that the resonance from water on gypsum was a doublet rather than a single broad signal. In a single crystal, the splitting between the doublet peaks varied with the angle with respect to the magnetic field and a powder sample gave the characteristic "Pake doublet", which provided an accurate measurement of the

internuclear distance [74, 75]. This is illustrated in Figure 1A for two situations [34]; on the left is the classic Pake doublet that results from the dipole-dipole coupling of two spin I=1/2 nuclei (^{1}H) in a rigid lattice; by contrast, on the right is a motionally averaged Pake doublet that results from the same two spins undergoing 180° rotation about an internal axis. The effect of the motion is to reduce the span of the powder pattern in half. Motion about other axes results in characteristic narrowing that can be related to the direction of the motion. This is an extremely useful phenomenon for characterizing intramolecular dynamics and, as discussed later in this article, for structure determination of membrane proteins by rotationally aligned (RA) solid-state NMR [28, 56, 76].

For all practical purposes, the development and application of NMR to solids and liquids proceeded along separate paths during the twenty-five year period from 1945 through 1970. With the introduction of programmable, pulsed Fourier transform instrumentation and dedicated instrument computers, both solution NMR and solid-state NMR methods were poised for rapid development in the 1970s. Because of the more difficult experiments and smaller community of experts in the field, solid-state NMR advanced more slowly than solution NMR. Now, since solution NMR of proteins is quite mature [12], and there have been dramatic strides in the instrumentation and experimental techniques of solid-state NMR of proteins [14, 20, 32, 41, 45, 48, 61, 62, 65, 72, 83, 91, 97, 100, 106, 107, 113, 118], the situation has reversed.

3.2 High-resolution solid-state NMR spectroscopy

A triad of methods constitutes the foundation of high-resolution solid-state NMR. These are multiple-pulse homonuclear decoupling of abundant spins (e.g., ^{1}H, ^{19}F) [111], combined cross-polarization and heteronuclear decoupling of dilute spins (*e.g.*, ^{13}C, ^{15}N) [86], and magic angle sample spinning to obtain single-line resonances from powder samples [2, 95]. All three methods have been greatly enhanced in capability since their introduction through improvements in instrumentation and experimental methods, and are now widely used. All three methods were introduced using ‘home-built’ equipment, and for some time that was the only way to perform the experiments, which limited their reach into the biochemical NMR community. However, modern commercial instruments are now capable of performing these highly demanding experiments remarkably well, enabling high-resolution solid-state NMR to have a much broader impact on chemistry and biochemistry.

In the seminal 1968 paper [111], Waugh and coworkers demonstrated a striking command of the nuclear spins with the first high-resolution NMR spectrum of a solid sample shown in Figure 2. Using the now-classic WaHuHa multiple-pulse experiment, they were able to attenuate the strong homonuclear couplings that were intractable to all previous approaches while preserving the chemical shift interaction. The resulting spectra had resonance line widths comparable to those of liquids in the same spectrometer, as shown by the comparison in the bottom spectrum in Figure 2. This demonstrated the key concept of selective averaging [37] of the effects of some spin-interactions while leaving one or a few others for analysis. This has gained its greatest applicability in multidimensional experiments, starting with separated local field (SLF) spectroscopy [38, 68, 112] of solids.

Significantly, among the first studies performed using multiple-pulse NMR on solids were those that characterized intramolecular dynamics [58]. The averaging of the ^{19}F chemical shift anisotropy powder pattern associated with a methyl group is shown in Figure 1B. At low temperatures rotation of the methyl group is not apparent in the chemical shift powder pattern, which is broad and non-axially symmetric. In contrast, at elevated temperatures where the methyl group does undergo rotation about its C3 axis, the resulting powder pattern is motionally averaged; characteristically it is axially symmetric and narrowed compared to the static powder pattern. Notably, the analogous experiment has been performed on the phospholipid [57] and protein [50] components of membranes.

Following the introduction of the original four-pulse WaHuHa experiment [111], there was an intense period of parallel development of the underlying coherent averaging theory [36] and more sophisticated experiments with improved compensation for imperfections in the pulses [37]. An important outcome of this era of solid-state NMR applications to chemistry was the determination of the ^{1}H chemical shift tensors of a wide variety of compounds [59].

The next innovation with far-reaching consequences for NMR applications to chemistry and biochemistry, also from Waugh and coworkers, was the introduction of proton-enhanced nuclear induction spectroscopy [85, 87]. The most elegant of experiments, cross-polarization of magnetization from the abundant bath of ^{1}H spins, with their relatively short T_1s, to the dilute ^{13}C or ^{15}N spins provides sensitivity enhancement, and the application of irradiation to the ^{1}H spins during data acquisition provides high resolution of the chemical shifts of the ^{13}C- or ^{15}N- containing compounds. The dramatic effects of this experiment on the ^{13}C NMR spectrum of a solid are shown in Figure 3. Notably, among the initial experiments, the effects of motional averaging on ^{13}C powder patters were demonstrated [87].

Solid-state NMR was fully brought into the realm of chemistry by combining magic angle sample spinning with cross-polarization and heteronuclear decoupling [95]. High-resolution spectra with distinguishable chemical shifts comparable to those obtained by dissolving the same polymers in solution are shown in Figure 4. This was a major step forward for the field, and is now widely applied to proteins. The instrumentation has undergone a remarkable amount of development, since the initial maximum spinning rates were 3 kHz and they are now greater than 100 kHz.

4. Solid-state NMR of proteins

Using home-built equipment, including machining our own stators and Andrew-Beams rotors, we obtained the first MAS solid-state NMR spectrum of a protein [69]. Even though the sample was natural abundance ^{13}C, with the use of large samples and extensive signal averaging it was feasible to resolve individual protein resonances. We also obtained the first ^{15}N MAS solid-state NMR spectrum of a protein [24]. This required an important step forward in isotopic labeling of proteins. Based on the famous Meselson-Stahl experiment[60], we noted that all of the molecules present in *E. coli* grown on minimal media where the sole source of nitrogen was ^{15}N-labeled ammonium sulfate had all of their ^{14}N replaced by ^{15}N. This provides uniformly ^{15}N labeled proteins, giving the necessary sensitivity for ^{15}N NMR spectroscopy. It is particularly convenient because there

are no nitrogens bonded to other nitrogens in proteins, making homonuclear ^{15}N-^{15}N decoupling unnecessary. It also opened the way for its use in solution NMR experiments [9], and was complemented by selective labeling by residue type for many classes of NMR experiments.

As shown in Figure 5 the triad of methods is highly effective for proteins in biological supramolecular structures, in this case our first examples, which were filamentous bacteriophages. These large rod-shaped particles give very broad and unresolved spectra using conventional solution NMR methods because of the lack of motional averaging. However, the combination of selective isotopic labeling, cross-polarization/heteronuclear decoupling, and magic angle sample spinning gives narrow single-line resonances [31].

It is feasible to determine the structures of crystalline globular proteins using MAS solid-state NMR, and this has been accomplished for spectrin [13], GB1 [117], Crh [51], ubiquitin [43], MMP-12 [7], and superoxide dismutase [47], among a growing number. Recently, the structure of a seven trans-membrane protein in phospholipids has been determined in this way [110].

5. Oriented sample solid-state NMR

Besides magic angle sample spinning, there is a second approach to obtaining high-resolution solid-state NMR spectra with single-line resonances, and that is the use of aligned samples. The archetypical example of an aligned sample, of course, is a single crystal, which gives single lines for each unique site in the unit cell. The one-dimensional spectrum at the top of Figure 6 is of a single crystal of calcium formate, illustrating the benefits of sample orientation in giving high resolution in the chemical shift dimension. Figure 6 also shows the first experimental two-dimensional separated local field spectrum [38]. Each signal associated with a ^{13}C bonded to a single ^{1}H is a doublet of the same origin as a Pake doublet [74]. In this case the local fields of the various carbon sites are separated by the chemical shifts of the carbon sites. The use of multiple pulse homonuclear decoupling separates the heteronuclear dipolar couplings from the complications of the multiple couplings throughout the large network of ^{1}H spins in the sample [112].

It is also the case that a single line resonance results from uniaxial alignment of a polymeric sample parallel to the direction of the magnetic field. This was originally illustrated with spectra of physically drawn (aligned) polyethylene [68]. There is only a single type of chemical group in polyethylene, thus only one signal. In the two-dimensional separated local field spectrum where the ^{1}H-^{13}C heteronuclear dipolar coupling is in one dimension and the ^{13}C chemical shift is in the second dimension, a triplet was observed due to the effects of the two hydrogens on the methylene groups of polyethylene.

A similar situation exists in Figure 7 where a single site is ^{15}N labeled in the major coat protein that is magnetically aligned and immobilized as part of a filamentous virus particle. The one-dimensional chemical shift spectra of an unoriented powder sample and a magnetically aligned sample of the filamentous bacteriophage fd are shown. Also shown is a two-dimensional SLF spectrum of the labeled residue. The finding of only a single resonance demonstrates that each protein subunit is arranged symmetrically in the

filamentous virus particle. The combination of the frequency of the single-line resonance and the heteronuclear dipolar splitting provide sufficient information to determine the position of the ^{15}N-labeled tryptophan side chain within the three-dimensional structure of the coat protein.

Figure 8 illustrates several of the key points necessary for developing a general method of structure determination using aligned samples. These samples of Pf1 filamentous bacteriophage were uniformly ^{15}N labeled by their growth in minimal media. The two SLF spectra were obtained at two different periods of the development of the method. Only half the dipolar coupling dimension is shown because it is symmetric about zero frequency, and this allows greater detail to be displayed. The spectrum in Figure 8b was obtained in 1983 [26] and only partial resolution could be achieved. In that era most of the substantial work required the use of selective isotopic labeling to provide resolution, assignment, and frequency measurements for individual sites. The spectrum in Figure 8c was obtained twenty years later [105]; the sample was essentially identical to that in Panel b. The great increase in resolution resulted from two main factors. One was the use of a higher field magnet, which served to spread the chemical shifts in one of the dimensions. The second was the implementation of polarization inversion spin exchange at the magic angle (PISEMA) [116], which provides much narrower lines in the dipolar coupling dimension than the original implementations of separated local field spectroscopy [38]. The combination of the two gives a striking improvement in the quality of the spectra. The spectrum in Figure 8c was fully assigned and the two orientationally-dependent frequencies associated with each resonance provided sufficient restraints for complete structure determination [105].

The same oriented sample method outlined above for single crystals, synthetic polymers and filamentous bacteriophages can be applied to membrane proteins. In oriented sample (OS) solid-state NMR of stationary, aligned samples of membrane proteins there are two approaches to sample alignment. One is mechanical alignment between glass plates [5, 23, 64] and the other is magnetic alignment using bicelles [42, 93], which are mixtures of long chain lipids that form the planar bilayer for the protein, with short chain lipids or detergents to ‘cap’ the ends of the bilayer region. Recently, we demonstrated that it is possible to prepare magnetically-alignable ‘detergent-free’ bicelles through the use of an amphipathic peptide instead of short chain lipids, which are referred to as macrodiscs [81].

Magnetic alignment enables the preparation of very highly aligned samples of membrane proteins [80]. This is illustrated in Figure 9 for membrane proteins with one, two, and seven trans-membrane helices. Figure 9D, E, and F are ^{31}P NMR spectra of the phospholipids that form the bilayers in the samples. The positions and line shapes of the resonances indicate that the bilayers are very highly aligned. The one-dimensional spectra in Figure 9A, B, and C are of the uniformly ^{15}N labeled samples of proteins embedded in the aligned bilayers. As can be seen for the smallest protein in Figure 9A, the resonance line widths are quite narrow. There is considerable spectral overlap in the results for the larger membrane proteins, although the underlying resonances are narrow.

The two-dimensional spectrum in Figure 9E is from the same sample used to obtain the one-dimensional spectra in Figure 9A and D. It displays excellent resolution in both the chemical shift and heteronuclear dipolar coupling dimensions, and, as marked, all of the resonances have been assigned to specific sites in the protein. The most noticeable feature is the "wheel-like" pattern of resonances, which comes from the trans-membrane helix. This is because of the regularity of the helix (residues 23 – 42) [54, 109], and these PISA (polarity index slant angle) wheels are extremely useful in the analysis of spectra of helical proteins.

6 Rotationally aligned solid-state NMR

Rotationally aligned (RA) solid-state NMR is specifically tailored for the unique properties of membrane proteins in liquid crystalline phospholipid bilayers. It combines features of magic angle spinning and oriented-sample solid-state NMR to resolve and assign resonances associated with each amino acid residue, measure site-specific orientation restraints relative to the bilayer, and calculate the three-dimensional structure of the protein and its orientation within the membrane bilayer. RA solid-state NMR differs from previously used OS solid-state NMR methods in that it relies on the inherent rotational diffusion of membrane proteins in phospholipid bilayers [17, 21] to provide orientation-dependent motional averaging of heteronuclear dipolar coupling and chemical shift anisotropy powder patterns relative to the bilayer normal, rather than the orientation-dependent frequencies of single-line resonances observed in OS NMR of stationary, uniaxially aligned samples. It differs from more standard MAS solid-state NMR approaches that typically rely on short-range distance and angle measurements within the polypeptide chain rather than to an externally defined axis, in this case the bilayer normal.

Phospholipids self-assemble to form extended bilayer membranes in liposomes. The polar head groups are exposed to water and the hydrophobic hydrocarbon chains face the membrane interior of the bilayer. On the molecular scale, these bilayers are infinitely long in two dimensions, but only two molecules thick in the third dimension. This is illustrated in Figure 10 by the representation of Singer and Nicholson's fluid mosaic model of a biological membrane [101]. Both the phospholipids and the proteins undergo fast rotational diffusion about the bilayer normal [15, 21], as indicated by the arrows, as well as translational diffusion in the plane of the bilayer.

The rotational diffusion of membrane proteins in phospholipid bilayers, illustrated in Figure 10, was shown to occur in the early 1970s by optical methods [15–19, 84, 90]. Notably, the same phenomenon was observed in the averaging of lineshapes by NMR. McLaughlin and coworkers in 1975 [57] used ^{31}P NMR of the phospholipids to show that they undergo fast rotational motion by two pertinent spectroscopic effects. One was the averaging of the powder pattern line shape and the other was the observation of single line spectra when the lipid bilayers were mechanically aligned on glass plates over a wide range of angles (not just with the normal parallel to the field). Ten years later, in a similar, complementary experiment Griffin and coworkers [50] demonstrated that the protein bacteriorhodopsin undergoes rotational diffusion in phosphatidyl choline bilayers because of the averaging of the $^{13}C'$ powder pattern, as illustrated in Figure 11A and B. Contemporarily, Cornell and coworkers [23, 102] showed that $^{13}C'$ labeled gramicidin undergoes the same type of

motional averaging in phospholipid bilayers. The results with ^{13}C labels in gramicidin [98] were confirmed with ^{2}H [49, 104] and ^{15}N labeled gramicidin; Cross and coworkers [30] showed that the ^{15}N powder pattern in an unoriented bilayer sample was axially symmetric, as required by motional averaging about the bilayer normal. In a highly definitive experiment, Cross and coworkers utilized gramicidin labeled at a single site to show with a two-dimensional SLF experiment that the motionally averaged chemical shift and dipolar coupling principal elements were collinear, while in a static sample they differ in alignment by about 17°. By obtaining narrow single-line resonances from protein-containing bicelles with their normals perpendicular to the magnetic field, we demonstrated that the membrane-bound form of fd coat protein undergoes rotational diffusion about the bilayer normal in phospholipid bilayers. In an even more definitive experiment, very similar to the original McLaughlin and coworkers experiment, we were able to show single line resonances from tilted coil samples over a wide range of angles, again something that could only be observed in the presence of rotational diffusion [78]. It was possible to take advantage of the angular dependence of the axially symmetric powder patterns to determine the tilt angle of a helix through the use of PISA wheels and Dipolar Wave that are based on the regularity of the secondary structure [79]. Subsequently, other groups determined the tilt angle of representatives of several classes of peptides by characterizing the rotationally averaged powder patterns of labeled sites [1, 11, 40, 63, 88]. In combination with magic angle spinning [6, 10, 28, 56, 76], the rotational alignment of membrane proteins enables complete resolution and measurement of motionally averaged ^{13}C and ^{15}N chemical shift anisotropies and ^{1}H-^{13}C and ^{1}H-^{15}N heteronuclear dipolar couplings. The spectral manifestations of rotational averaging provide the experimental foundation for RA solid-state NMR.

In the structure determination of membrane proteins by RA solid-state NMR, it is essential to verify that the protein undergoes rapid rotational diffusion about the bilayer normal and that this rotation can be switched between slow and fast limit by changing the temperature. As shown in Figure 11, it is particularly convenient to monitor the effect of temperature on the $^{13}C'$ CSA powder pattern of a uniformly $^{13}C/^{15}N$ labeled membrane protein in proteoliposomes [50]. This powder pattern line shape is effective in demonstrating that a helical membrane protein is undergoing fast rotational diffusion, since the static powder pattern is highly asymmetric with a large frequency span. For transmembrane helices a large fraction of the backbone carbonyl bonds are approximately parallel to the bilayer normal (*i.e.*, the axis of motional averaging); thus, when the protein undergoes fast rotational diffusion, the $^{13}C'$ powder pattern becomes axially symmetric and is significantly narrowed. This is shown in Figure 11 with experimental data from the protein MerFt in DMPC bilayers [28]. A useful way to experimentally monitor the protein rotational diffusion is with slow (5 kHz) MAS as shown in Figure 11E (fast rotational diffusion of the protein) and Figure 11F (slow rotational diffusion of the protein). There is a family of sidebands when the $^{13}C'$ CSA has its full static breadth; in contrast, the motionally averaged CSA has such a small span that there are no observable spinning sidebands, even at the 5 kHz rate.

The full two-dimensional ^{1}H-^{15}N dipolar coupling/^{13}C chemical shift SLF spectrum shown in Figure 12A contains resonances from all of MerFt's $^{13}C\alpha$ sites. Although there is considerable spectral overlap, an individual resonance assigned to Leu 31 can be identified,

as marked in Figure 12A. The rotationally averaged ^{1}H-^{15}N dipolar coupling and ^{15}N CSA powder patterns associated with each isotropic resonance are characterized with three-dimensional MAS solid-state NMR experiments. Figure 12B and C contains two-dimensional ^{1}H-^{15}N dipolar coupling/^{13}C chemical shift planes selected from a three-dimensional spectrum at the ^{15}N shift frequency corresponding to Leu 31. ^{1}H-^{13}C heteronuclear dipolar couplings were measured with similar three-dimensional experiments (Figure 12C). Since we previously verified [76] that the measurement of orientation-dependent frequencies from the parallel edges of the recoupled, motionally averaged, axially symmetric powder patterns[74] are identical to those measured from the single line resonances observed in aligned, stationary samples, the frequencies measured from the spectra in Figure 12 can be used to determine the orientation of the peptide plane for Leu 31 and, in general, with sufficient data from other residues, to calculate the three-dimensional structure of the protein [28].

The frequencies measured from the spectra in Figure 12 are interpreted graphically in Figure 13. The experimentally measured, motionally averaged ^{1}H-^{13}C and ^{1}H-^{15}N heteronuclear dipolar couplings are compared to calculated static powder patterns on the right side of the Figure. On the left side, the resulting angular vectors derived from the experimental data are superimposed on the peptide plane of Leu 31.

The ^{1}H-^{15}N and ^{1}H-$^{13}C\alpha$ dipolar coupling restraints and ^{15}N chemical shift anisotropy restraints are sufficient to determine the orientation of the associated peptide plane relative to the axis of alignment and yield the three-dimensional structure of the protein. The protocol [56] for calculating protein structures from OS solid-state NMR data is outlined in Figure 14. It relies on a fragment based approach in the initial stage using the program Rosetta[29], and then full refinement in performed with all experimental restraints using the program XPLOR-NIH[96]. It was followed to determine the structures of the three membrane proteins shown in Figures 15 – 18.

7. Applications to membrane proteins

7a. MerF

Mercury transport membrane proteins from the bacterial mercury detoxification system [3] transport ionic Hg(II) from the periplasmic protein, MerP [103], across the hydrophobic bilayer, to the cytoplasmic enzyme, MerA, which reduces the extremely toxic Hg(II) to the much less toxic and volatile metallic form of mercury, Hg(0) [44]. We determined the structure of one of the mercury transport proteins, MerF, in phospholipid bilayers by RA solid-state NMR [52], ensuring that it is in its physiologically active state. The 81-residue MerF has two transmembrane helices and two Hg(II) binding sites, which contain pairs of cysteine residues [114]. The structure of MerF in phospholipid bilayers determined by solid-state NMR spectroscopy is shown in Figure 15.

The structure determined by RA solid-state NMR reveals two crucial aspects of MerF, one of which is of general importance to the structure determination and analysis of membrane proteins. The second is that the juxtaposition of the two Hg(II) binding sites, identified with arrows in Figure 15, suggests a plausible mechanism for the transport of the Hg(II) ions

across the hydrophobic bilayers. We also determined the structure of an N- and C- terminal truncated construct of MerF (MerFt) and found it to have a remarkably different structure (Figure 16). The terminal residues of full-length MerF are mobile and unstructured in micelles, but are structured in the full-length and truncated forms of the protein in phospholipid bilayers. However, a substantial portion of the protein is different in the comparison of the full-length and truncated forms. These findings show that even fairly conservative alterations of the amino acid sequence can have profound effects on the folding of membrane proteins, and that detergent micelles can significantly alter the structure of the same polypeptide sequence. This is also apparent in Figure 17 with the comparison of the structures of p7 in micelles and bilayers.

The superposition of the structures of the full-length (aqua) and truncated (magenta) protein structures in Figure 16 is highly informative. The truncation of the N-terminal residues, which are mobile and unstructured in micelles, results in a dramatic rearrangement of the amphipathic helix (Ile 13 – Pro 25). These residues change from an orientation perpendicular to the bilayer normal to one that is nearly parallel to the bilayer normal and appears to be a continuation of the first transmembrane helix that extends out of the bilayer. Both structures were determined using identical sample conditions and methods; therefore, the observed structural rearrangement results solely from the alteration of the amino acid sequence of the protein. In contrast to the N-terminal truncation the C-terminal truncation does not appear to cause significant structural changes. These observations suggest caution in the use of truncations and other protein modifications of membrane proteins.

A key question in the study of the mercury transport mechanism is the location of the N-terminal Hg(II) binding site, which is shown in Figure 15 to be in close proximity to the second Hg(II) binding site, which is located near the bilayer's hydrophobic to hydrophilic interface. Previous biochemical studies and predictions on various mercury transporter proteins are inconsistent in identifying the location of the N-terminal binding site, ranging from the interface on the cytosolic side to the middle of the first membrane helix. The structure in Figure 15 supports the existence of the former topology. The second important observation is the proximity of the two metal binding sites on MerF, which supports the possibility of direct intramolecular Hg(II) transfers. Notably, the existence of direct contact has been hypothesized from various studies on mercury ligand exchange and mercury coordination chemistry. In any transport mechanism, tight control of Hg(II) is essential because of its high reactivity in solution, and the only way to transfer Hg(II) while maintaining tight control is through direct contact and ligand exchange between Hg(II) binding sites.

7b. p7

Hepatitis C virus (HCV) is an enveloped virus [53] with an RNA genome that is translated into a single 3000-residue polyprotein, which is cleaved by cellular and viral proteases to yield ten proteins [92]. One of the proteins, p7, is a small viral protein whose gene is located between those for the proteins that constitute the structural core and those for the non-structural proteins. p7 is essential for efficient virus particle assembly and release but not RNA replication. p7 has 63 residues, two trans-membrane helices, and appears to be a

hexamer by electron microscopy[23], which may account for its channel activity. However, its biological roles are likely to be more numerous and multifaceted than simply acting as an ion channel. Indeed, its channel activity may be secondary to its principal biological activities of interacting with other proteins.

The structure of p7 is of interest in its own right, since the protein plays key roles in the viral lifecycle and is a potential drug target. It is also a prime example of a protein whose structure is affected by its environment. It is important to acknowledge the uncertainties associated with studying membrane proteins in any membrane-mimicking environment other than liquid crystalline phospholipid bilayers. We have determined the structure of p7 in DHPC micelles by solution NMR [22] and in DMPC bilayers by RA solid-state NMR. Both structures indicate that p7 is a remarkably complex protein considering that it has only 63 residues and its secondary structure is dominated by two hydrophobic trans-membrane helices. Another structure of p7 in micelles shows structural complexity as well [73]. The comparison of structures in Figure 17 suggests that the structural distortions result from the hydrophobic helices being stabilized by the hydrophobic environment at the center of the micelle. Regardless, of the reason, the structure in phospholipid bilayers is likely to be more representative of the in vivo structure of the protein. This is a factor to be taken into account with all membrane proteins that is being thoroughly analyzed by Cross and coworkers [27, 119].

7c. CXCR1

CXCR1 is a class A rhodopsin-like G-protein coupled receptor for the chemokine interleukin-8 (IL-8), which mediates the immune and inflammatory responses associated with many disease states [39], including tumor growth and lung inflammation. The structure of CXCR1 shares significant similarities with that of CXCR4, the only other chemokine receptor whose structure has been determined [115], and it is of interest to identify structural differences due to variations in the amino acid sequences of the two proteins. However, the most notable structural differences appear to be associated with changes in the amino acid sequence of CXCR4 necessitated by the requirements of crystallization, and possibly the use of monoolein as the surrounding detergent, rather than a phospholipid bilayer. The changes in the sequence of CXCR4 include the insertion of T4 lysozyme in intracellular loop 3, removal of 33 C-terminal residues, and a site-specific mutation. There are structural differences throughout the proteins, especially in the vicinity of the sequence changes.

As seen in the representations in Figure 18, the CXCR1 helices are well defined by the NMR data [82]. For example, the data show the presence of a kink that changes the direction of trans-membrane helix 2 (residues 74 – 101) at Phe 88. The extracellular beginning of trans-membrane helix 7, just after extracellular loop 3, is tilted towards the central axis of the receptor. Residues immediately preceding the mobile C terminus form a well-defined helix (helix 8; residues Gln 310 through Ala 321). Helix 8 has a distinctly amphipathic amino acid sequence, and aligns along the membrane surface, indicating that the phospholipid bilayer may have a role in its adopting a helical structure at the membrane to aqueous interface. The NMR data also show the presence of two disulfide bonds, which are

highly conserved in this class of GPCRs that are important for ligand binding and play roles in forming the extracellular structure of the receptor.

The charged residues are located mainly near the membrane-water interface with negative charges clustered in the extracellular loops. In addition, four charged residues, contributed by trans-membrane helix 2 (Asp 85), trans-membrane helix 3 (Lys 117), and trans-membrane helix 7 (Asp 288 and Glu 291), form a polar cluster in the core of the helical bundle that may have effects on ligand binding and receptor signaling. The intracellular loops are crucial for G-protein interactions, and are well defined in the structure determined by RA solid-state NMR.

8. A view to the future of solid-state NMR of membrane proteins

The structures of only a limited number of domains or full-length proteins have been determined in phospholipid bilayers; these include gramicidin [46], the M2 channel forming membrane segment of the acetylcholine receptor [70], the membrane-bound form of fd coat protein [55], the channel forming membrane segment of Vpu from HIV [77], the channel forming membrane segment of the influenza M2 protein [11, 99], N- and C- terminal truncated MerF [28], full-length MerF [52], CXCR1 [82], a sensory rhodopsin [110], and p7 from HCV. Improvements in instrumentation, experimental methods, and calculation methods are starting to have a large impact on the field. The pace and quality of structure determination of membrane proteins by solid-state NMR is improving rapidly. The spectroscopy is firmly based in some of the earliest work in the field. The ability to determine the structures of unmodified membrane proteins in liquid crystalline phospholipid bilayers under physiological conditions of temperature and pH is an enormous advantage over competitive methods. There is every reason to believe that solid-state NMR will become a standard method for determining the structures of membrane proteins in the future.

Acknowledgments

We thank Jasmina Radoicic for editorial assistance. The research described in this review that was performed at the University of California, San Diego was supported by Grants R01GM066978, RO1EB005161, and R01GM099986 from the National Institutes of Health. It utilized the Biomedical Technology Resource for NMR Molecular Imaging of Proteins at the University of California, San Diego supported by P41EB002031.

Abbreviations

CSA	chemical shift anisotropy
GPCR	G-protein coupled receptor
I spin	abundant spin, e.g., ^{1}H or ^{19}F
MAS	magic angle spinning
NMR	nuclear magnetic resonance
OS	oriented sample
PISEMA	polarization inversion spin exchange at the magic angle

RA	rotationally aligned
S spin	dilute spin, e.g., ^{13}C or ^{15}N
SLF	separated local field

References

1. Aisenbrey C, Bechinger B. Investigations of polypeptide rotational diffusion in aligned membranes by 2H and 15N solid-state NMR spectroscopy. J Am Chem Soc. 2004; 126:16676–16683. [PubMed: 15600374]
2. Andrew ER, Bradbury A, Eades RG. Nuclear magnetic resonance spectra from a crystal rotated at high speed. Nature. 1958; 182:1659.
3. Barkay T, Miller SM, Summers AO. Bacterial mercury resistance from atoms to ecosystems. FEMS Microbiol Rev. 2003; 27:355–384. [PubMed: 12829275]
4. Bauer DR, Opella SJ, Nelson DJ, Pecora R. Depolarized light scattering and carbon nuclear resonance measurements of the isotropic rotational correlation time of muscle calcium binding protein. J Am Chem Soc. 1975; 97:2580–2582. [PubMed: 1133427]
5. Bechinger B, Kim Y, Chirlian LE, Gesell J, Neumann JM, Montal M, Tomich J, Zasloff M, Opella SJ. Orientations of amphipathic helical peptides in membrane bilayers determined by solid-state NMR spectroscopy. J Biomol NMR. 1991; 1:167–173. [PubMed: 1726781]
6. Bechinger B, Aisenbrey C, Bertani P. The alignment, structure and dynamics of membrane-associated polypeptidess by solid-state NMR spectroscopy. Biochim Biophys Acta. 2004; 1666:190–204. [PubMed: 15519315]
7. Bertini I, Bhaumik A, DePaepe G, Griffin RG, Lelli M, Lewandowski JR, Luchinat C. High-resolution solid-state NMR structure of a 17.6 kDa protein. J Am Chem Soc. 2010; 132:1032–1040. [PubMed: 20041641]
8. Bloch F, Hansen WW, Packard M. The nuclear induction experiment. Physical Review. 1946; 70:474–485.
9. Bogusky MJ, Tsang P, Opella SJ. One- and two- dimensional 15N/1H NMR of filamentous phage coat proteins in solution. Biochem Biophys Res Commun. 1985; 127:540–545. [PubMed: 3977936]
10. Cady SD, Hong M. Simultaneous extraction of multiple orientational constraints of membrane proteins by 13C-detected N-H dipolar couplings under magic angle spinning. J Magn Reson. 2008; 191:219–225. [PubMed: 18221902]
11. Cady SD, Schmidt-Rohr K, Wang J, Soto CS, Degrado WF, Hong M. Structure of the amantadine binding site of influenza M2 proton channels in lipid bilayers. Nature. 2010; 463:689–692. [PubMed: 20130653]
12. Campbell ID. The evolution of protein NMR. Biomedical Spectroscopy and Imaging. 2013; 2:245–264.
13. Castellani F, van Rossum B, Diehl A, Schubert M, Rehbein K, Oschkinat H. Structure of a protein determined by solid-state magic-angle-spinning NMR spectroscopy. Nature. 2002; 420:98–102. [PubMed: 12422222]
14. Cegelski L. REDOR NMR for drug discovery. Bioorg Med Chem Lett. 2013; 23:5767–5775. [PubMed: 24035486]
15. Cherry RJ. Protein mobility in membranes. FEBS Lett. 1975; 55:1–7. [PubMed: 237788]
16. Cherry RJ, Muller U, Schneider G. Rotational diffusion of bacteriorhodopsin in lipid membranes. FEBS Lett. 1977; 80:465–469. [PubMed: 891998]
17. Cherry RJ. Measurement of protein rotational diffusion in membranes by flash photolysis. Methods Enzymol. 1978; 54:47–61. [PubMed: 215879]
18. Cherry RJ. Rotational and lateral diffusion of membrane proteins. Biochim Biophys Acta. 1979; 559:289–327. [PubMed: 391281]

19. Cherry RJ, Godfrey RE. Anisotropic rotation of bacteriorhodopsin in lipid membranes: Comparison of theory with experiment. Biophys J. 1981; 36:257–276. [PubMed: 7284552]
20. Comellas G, Rienstra CM. Protein structure determination by magic-angle spinning solid-state NMR, insights into the formation structure, and stability of amyloid fibrils. Annu Rev Biophys. 2013; 42:515–536. [PubMed: 23527778]
21. Cone RA. Rotational diffusion of rhodopsin in the visual receptor membrane. Nature New Biology. 1972; 236:39–43.
22. Cook GA, Dawson LA, Tian Y, Opella SJ. Three-dimensional structure and interaction studies of Hepatitis C Virus p7 in 1,2-dihexanoyl-sn-glycero-3-phospholcholine by solution nuclear magnetic resonance. Biochemistry. 2013; 52:5295–5303. [PubMed: 23841474]
23. Cornell BA, Separovic F, Smith R, Baldassi AJ. Conformation and orientation of gramicidin A in oriented phospholipid bilayers measured by solid state carbon-13 NMR. Biophys J. 1988; 53:67–76. [PubMed: 19431717]
24. Cross TA, DiVerdi JA, Opella SJ. Strategy for nitrogen NMR of biopolymers. J Am Chem Soc. 1982; 104:1759–1761.
25. Cross TA, Opella SJ. Protein structure by solid state NMR. J Am Chem Soc. 1983; 105:306–308.
26. Cross TA, Tsang P, Opella SJ. Comparison of protein and deoxyribonucleic acid backbone structures in fd and Pf1 bacteriophages. Biochemistry. 1983; 22:721–726. [PubMed: 6340725]
27. Cross TA, Murray DT, Watts A. Helical membrane protein conformations and their environment. European biophysics journal: EBJ. 2013; 42:731–755. [PubMed: 23996195]
28. Das BB, Nothnagel HJ, Lu GJ, Son WS, Tian Y, Marassi FM, Opella SJ. Structure determination of a membrane protein in proteoliposomes. J Am Chem Soc. 2012; 134:2047–2056. [PubMed: 22217388]
29. Das R, Baker D. Macromolecular modeling with Rosetta. Annual Review of Biochemistry. 2008; 77:363–382.
30. Fields GB, Fields CG, Petefish J, Van Wart HE, Cross TA. Solid-phase peptide synthesis and solid-state NMR spectroscopy of [Ala3-15N][Val1]gramicidin A. Proceedings of the National Academy of Sciences of the United States of America. 1988; 85:1384–1388. [PubMed: 2449690]
31. Gall CM, Cross TA, DiVerdi JA, Opella SJ. Protein dynamics by solid-state NMR: aromatic rings of the coat protein in fd bacteriophage. Proc Natl Acad Sci U S A. 1982; 79:101–105. [PubMed: 6948294]
32. Goncalves JA, Eilers M, South K, Opefi CA, Laissue P, Reeves PJ, Smith SO. Magic angle spinning nuclear magnetic resonance spectroscopy of G protein-coupled receptors. Meth Enzymol. 2013; 522:365–389. [PubMed: 23374193]
33. Gutowsky HS, Kistiakowsky GB, Pake GE, Purcell EM. Structural investigations by means of nuclear magnetism. I. Rigid crystal lattices. J Chem Phys. 1949; 17:972–981.
34. Gutowsky HS, Pake GE. Structural investigations by means of nuclear magnetism. II. Hindered rotation in solids. J Chem Phys. 1950; 18:162–170.
35. Gutowsky HS, Pake GE, Bersohn R. Structural investigations by means of nuclear magnetism. III. Ammonium halides. J Chem Phys. 1954; 22:643.
36. Haeberlen U, Waugh JS. Coherent averaging effects in magnetic resonance. Phys Rev. 1968; 175:453–467.
37. Haeberlen U. High resolution NMR in solids. Selective averaging. Advances in Magnetic Resonance. 1976; (Supplement 1):1–190.
38. Hester RK, Ackerman JL, Neff BL, Waugh JS. Separated local field spectra in NMR: determination of structure of solids. Phys Rev Lett. 1976; 36:1081–1083.
39. Holmes WE, Lee J, Kuang WJ, Rice GC, Wood WI. Structure and functional expression of a human interleukin-8 receptor. Science. 1991; 253:1278–1280. [PubMed: 1840701]
40. Hong M, Doherty T. Orientation determination of membrane-disruptive proteins using powder samples and rotational diffusion: A simple solid-state NMR approach. Chem Phys Lett. 2006; 432:296–300. [PubMed: 17364006]
41. Hong M, Zhang Y, Hu F. Membrane protein structure and dynamics from NMR spectroscopy. Annual review of physical chemistry. 2012; 63:1–24.

42. Howard KP, Opella SJ. High-resolution solid-state NMR spectra of integral membrane proteins reconstituted into magnetically oriented phospholipid bilayers. J Magn Reson B. 1996; 112:91–94. [PubMed: 8661314]
43. Huber M, Hiller S, Schanda P, Ernst M, Bockmann A, Verel R, Meier BH. A proton-detected 4D solid-state NMR experiment for protein structure determination. ChemPhyschem. 2011; 12:915–918. [PubMed: 21442705]
44. Johs A, Harwood JM, Parks JM, Nauss RE, Smith JC, Liang L, Miller SM. Structural characterization of intramolecular Hg(II) transfer between flexibily linked domains of mercuric ion reductase. J Mol Biol. 2011; XX web published.
45. Judge PJ, Watts A. Recent contributions from solid-state NMR to the understanding of membrane protein structure and function. Curr Opin Chem Biol. 2011; 15:690–695. [PubMed: 21862384]
46. Ketchem RR, Hu W, Cross TA. High-resolution conformation of gramicidin A in a lipid bilayer by solid-state NMR. Science. 1993; 261:1457–1460. [PubMed: 7690158]
47. Knight MJ, Pell AJ, Bertini I, Felli IC, Gonnelli L, Pierattelli R, Herrmann T, Emsley L, Pintacuda G. Structure and backbone dynamics of a microcrystalline metalloprotein by solid-state NMR. Proc Natl Acad Sci. 2012; 109:11095–11100. [PubMed: 22723345]
48. Knight MJ, Felli IC, Pierattelli R, Emsley L, Pintacuda G. Magic angle spinning NMR of paramagnetic proteins. Accounts of chemical research. 2013; 46:2108–2116. [PubMed: 23506094]
49. Lee KC, Hu W, Cross TA. 2H NMR determination of the global correlation time of the gramicidin channel in a lipid bilayer. Biophys J. 1993; 65:1162–1167. [PubMed: 7694670]
50. Lewis BA, Harbison GS, Herzfeld J, Griffin RG. NMR structural analysis of a membrane protein: bacteriorhodopsin peptide backbone orientation and motion. Biochemistry. 1985; 24:4671–4679. [PubMed: 4063350]
51. Loquet A, Bardiaux B, Gardiennet C, Blanchet C, Baldus M, Nilges M, Malliavian T, Bockmann A. 3D structure determination of the Crh protein from highly ambiguous solid-state NMR restraints. J Am Chem Soc. 2008; 130:3579–3589. [PubMed: 18284240]
52. Lu GJ, Tian Y, Vora N, Marassi FM, Opella SJ. The Structure of the Mercury Transporter MerF in Phospholipid Bilayers: A Large Conformational Rearrangement Results from N-Terminal Truncation. J Am Chem Soc. 2013; 135:9299–9302. [PubMed: 23763519]
53. Major ME, Feinstone SM. The molecular virology of hepatitis C. Hepatology. 1997; 25:1527–1538. [PubMed: 9185778]
54. Marassi FM, Opella SJ. A solid-state NMR index of helical membrane protein structure and topology. J Magn Reson. 2000; 144:150–155. [PubMed: 10783285]
55. Marassi FM, Opella SJ. Simultaneous assignment and structure determination of a membrane protein from NMR orientational restraints. Protein Sci. 2003; 12:403–411. [PubMed: 12592011]
56. Marassi FM, Das BB, Lu GJ, Nothnagel HJ, Park SH, Son WS, Tian Y, Opella SJ. Structure determination of membrane proteins in five easy pieces. Methods. 2011; 55:363–369. [PubMed: 21964394]
57. McLaughlin AC, Cullis PR, Hemminga MA, Hoult DI, Radda GK, Ritchie GA, Seeley PJ, Richards RE. Application of 31P NMR to model and biological membrane systems. FEBS Lett. 1975; 57:213–218. [PubMed: 1175790]
58. Mehring M, Griffin RG, Waugh JS. 19F Shielding tensors from coherently narrowed NMR powder spectra. J Chem Phys. 1971; 55:746–755.
59. Mehring, M. Principles of high resolution NMR in solids. 2. Springer-Verlag; 1983. p. 1-342.
60. Meselson M, Stahl F. The replication of DNA in Escherichia coli. Proc Natl Acad Sci. 1958; 44:671–682. [PubMed: 16590258]
61. Mueller LJ, Dunn MF. Crystallography of Enzyme Active Sites: Probing Chemically-Detailed, NMR Three-Dimensional Structure in Tryptophan Synthase. Accounts of chemical research. 2013; 46:2008–2017. [PubMed: 23537227]
62. Murray DT, Das N, Cross TA. Solid state NMR strategy for characterizing native membrane protein structures. Accounts of chemical research. 2013; 46:2172–2181. [PubMed: 23470103]
63. Naito A. Structure elucidation of membrane-associated peptides and proteins in oriented bilayers by solid-state NMR spectroscopy. Solid State Nuclear Magnetic Resonance. 2009; 36:67–76. [PubMed: 19647984]

64. Nicholson LK, Moll F, Mixon TE, LoGrasso PV, Lay JC, Cross TA. Solid-state 15N NMR of oriented lipid bilayer bound gramicidin A′. Biochemistry. 1987; 26:6621–6626. [PubMed: 2447939]

65. Opella S. Structure determination of membrane proteins by nuclear magnetic resonance spectrocopy. Annu Rev Anal Chem. 2013; 6:305–328.

66. Opella SJ, Nelson DJ, Jardetzyk O. Carbon magnetic resonance study of the conformational changes in carp muscle calcium binding parvalbumin. J Am Chem Soc. 1974; 96:7157–7159. [PubMed: 4474190]

67. Opella SJ, Yesinowski JP, Waugh JS. Nuclear magnetic resonance description of molecular motion and phase separations of cholesterol in lecithin dispersions. Proc Natl Acad Sci U S A. 1976; 73:3812–3815. [PubMed: 1069266]

68. Opella SJ, Waugh JS. Two-dimensional 13C NMR of highly oriented polyethylene. J Chem Phys. 1977; 66:4919–4924.

69. Opella SJ, Frey MH, Cross TA. Detection of individual carbon resonances in solid proteins. J Am Chem Soc. 1979; 101:5856–5857.

70. Opella SJ, Marassi FM, Gesell JJ, Valente AP, Kim Y, Oblatt-Montal M, Montal M. Structures of the M2 channel-lining segments from nicotinic acetylcholine and NMDA receptors by NMR spectroscopy. Nat Struct Biol. 1999; 6:374–379. [PubMed: 10201407]

71. Opella SJ, Zeri AC, Park SH. Structure dynamics and assembly of filamentous bacteriophages by nuclear magnetic resonance spectroscopy. Annu Rev Phys Chem. 2008; 59:635–657. [PubMed: 18393681]

72. Opella SJ. Structure determination of membrane proteins in their native phospholipid bilayer environment by rotationally aligned solid-state NMR spectroscopy. Accounts of chemical research. 2013; 46:2145–2153. [PubMed: 23829871]

73. OuYang B, Xie S, Berardi MJ, Zhao X, Dev J, Yu W, Sun B, Chou JJ. Unusual architecture of the p7 channel from hepatitis C virus. Nature. 2013; 498:521–525. [PubMed: 23739335]

74. Pake GE. Nuclear Resonance Absorption in Hydrated Crystals: Fine Structure of the Proton Line. The Journal of Chemical Physics. 1948; 16:327–336.

75. Pake GE, Purcell EM. Line shapes in nuclear paramagnetism. Phys Rev. 1948; 74:1184–1190.

76. Park S, Das BB, DeAngelis AA, Scrima M, Opella SJ. Mechanically, magnetically, and ‘rotationally aligned’ membrane proteins in phospholipid bilayers give equivalent angular constraints for NMR structure determination. J Phys Chem B. 2010; 114:13995–13003. [PubMed: 20961141]

77. Park SH, Mrse AA, Nevzorov AA, Mesleh MF, Oblatt-Montal M, Montal M, Opella SJ. Three-dimensional structure of the channel-forming trans-membrane domain of virus protein “u” (Vpu) from HIV-1. J Mol Biol. 2003; 333:409–424. [PubMed: 14529626]

78. Park SH, Mrse AA, Nevzorov AA, De Angelis AA, Opella SJ. Rotational diffusion of membrane proteins in aligned phospholipid bilayers by solid-state NMR spectroscopy. J Magn Reson. 2005; 178:162–165. [PubMed: 16213759]

79. Park SH, Opella SJ. Tilt angle of a trans-membrane helix is determined by hydrophobic mismatch. J Mol Biol. 2005; 350:310–318. [PubMed: 15936031]

80. Park SH, Opella SJ. Triton X-100 as the ‘short-chain lipid’ improves the magentic alignment and stability of membrane proteins in phosphatidylcholine bilayers for oriented-sample solid-state NMR spectroscopy. J Am Chem Soc. 2010; 132:12552–12553. [PubMed: 20735058]

81. Park SH, Berkamp S, Cook G, Chan MK, Viadiu H, Opella SJ. Nanodiscs vs. Macrodiscs for NMR of membrane proteins. Biochemistry. 2011; 50:8983–8985. [PubMed: 21936505]

82. Park SH, Das BB, Casagrande F, Tian Y, Nothnagel HJ, Chu M, Kiefer H, Maier K, De Angelis AA, Marassi FM, Opella SJ. Structure of the chemokine receptor CXCR1 in phospholipid bilayers. Nature. 2012; 7426:779–783. [PubMed: 23086146]

83. Parthasarathy S, Nishiyama Y, Ishii Y. Sensitivity and resolution enhanced solid-state NMR for paramagnetic systems and biomolecules under very fast magic angle spinning. Accounts of chemical research. 2013; 46:2127–2135. [PubMed: 23889329]

84. Peters R, Cherry RJ. Lateral and rotational diffusion of bacteriorhodopsin in lipid bilayers: Experimental test of the Saffman-Delbruck equations. Proc Natl Acad Sci. 1982; 79:4317–4321. [PubMed: 6956861]

85. Pines A, Gibby MG, Waugh JS. Proton-enhanced nuclear induction spectroscopy. 13C chemical shielding anisotropy in some organic solids. Chemical Physics Letters. 1972; 15:373–376.

86. Pines A, Gibby MG, Waugh JS. Proton-enhanced nuclear induction spectroscopy - method for high-resolution NMR of dilute spins in solids. J Chem Phys. 1972; 56:1776–1777.

87. Pines A, Gibby MG, Waugh JS. Proton-enhanced NMR of dilute spins in solids. J Chem Phys. 1973; 59:569–590.

88. Prongidi-Fix L, Bertani P, Bechinger B. The membrane alignment of helical peptides from non-oriented 15N chemical shift solid-state NMR spectroscopy. J Am Chem Soc. 2007; 129:8430–8431. [PubMed: 17571892]

89. Purcell EM, Torrey HC, Pound RV. Resonance absorption by nuclear magnetic moments in a solid. Physical Review Letters. 1946:37–38.

90. Razi Naqvi K, Gonzalaz-Rodriguez J, Cherry RJ, Chapman D. Spectroscopic technique for studying protein rotation in membranes. Nature New Biology. 1973; 245:249–251.

91. Saito H, Ando I, Ramamoorthy A. Chemical shift tensor - The heart of NMR: Insights into biological aspects of proteins. Prog NMR Spec. 2010; 57:181–228.

92. Sakai A, Clairfe MS, Faulk K, Govindarajan S, Emerson SU, Purcell RH, Bukh J. The p7 polypeptide of hepatitis C virus is critical for infectivity and contins functionally important genotype-specific sequences. Proc Natl Acad Sci. 2007; 100:12712–12716.

93. Sanders CR, Hare BJ, Howard KP, Prestegard JH. Magnetically-oriented phospholipid micelles as a tool for the study of membrane-associated molecules. Progress in Nuclear Magnetic Resonance Spectroscopy. 1994; 26:421–444.

94. Saunders M, Wishnia A, Kirkwood JG. The nuclear magnetic resonance spectrum of ribonuclease. J Am Chem Soc. 1957; 79:3289–3290.

95. Schaefer J, Stejskal EO. C-13 Nuclear Magnetic Resonance of Polymers Spinning At the Magic Angle. J Am Chem Soc. 1976; 98:1031–1032.

96. Schwieters CD, Kuszewski JJ, Tjandra N, Clore GM. The Xplor-NIH NMR molecular structure determination package. Journal of Magnetic Resonance. 2003; 160:65–73. [PubMed: 12565051]

97. Sengupta I, Nadaud PS, Jaroniec CP. Protein structure determination with paramagnetic solid-state NMR spectroscopy. Accounts of chemical research. 2013; 46:2117–2126. [PubMed: 23464364]

98. Separovic F, Pax R, Cornell BA. NMR order parameter analysis of a peptide plane aligned in a lyotropic liquid crystal. Molec Phys. 1993; 78:357–369.

99. Sharma M, Yi M, Dong H, Qin H, Peterson E, Busath DD, Zhou HX, Cross TA. Insight into the mechanism of the influenza A proton channel from a structure in a lipid bilayer. Science. 2010; 330:509–512. [PubMed: 20966252]

100. Shi L, Ladizhansky V. Magic angle spinning solid-state NMR experiments for structural characterization of proteins. Methods Mol Biol. 2012; 895:153–165. [PubMed: 22760319]

101. Singer SJ, Nicholson GL. The fluid mosaic model of the structure of cell membranes. Science. 1972; 175:720–731. [PubMed: 4333397]

102. Smith R, Cornell BA. Dynamics of the intrinsic membrane polypeptide gramicidin A in phospholipid bilayers. Biophys J. 1986; 49:117–118. [PubMed: 19431611]

103. Steele RA, Opella SJ. Structures of the reduced, mercury-bound forms of MerP, the periplasmic protein from the bacterial mercury detoxification system. Biochemistry. 1997; 36:6885–6895. [PubMed: 9188683]

104. Strandberg E, Ozdirekcan S, Rijkers DT, van der Wel PC, Koeppe RE, Liskamp RM, Killian JA. Tilt angles of transmembrane model peptides in oriented and non-oriented lipid bilayers as determined by 2H solid-state NMR. Biophys J. 2004; 86:3709–3721. [PubMed: 15189867]

105. Thiriot DS, Nevzorov AA, Zagyanskiy L, Wu CH, Opella SJ. Structure of the coat protein in Pf1 bacteriophage determined by solid-state NMR spectroscopy. J Mol Biol. 2004; 341:869–879. [PubMed: 15288792]

106. Ullrich SJ, Glaubitz C. Perspectives in enzymology of membrane proteins by solid-state NMR. Accounts of chemical research. 2013; 46:2164–2171. [PubMed: 23745719]

107. Ulrich AS. Solid state 19G NMR methods for studying biomembranes. Prog Nucl Magn Reson Spectrosc. 2005; 46:1–21.

108. Urbina J, Waugh JS. Application of proton-enhanced nuclear induction spectroscopy to the study of membranes. Ann NY Acad Sci. 1973; 222:733–739. [PubMed: 4594299]

109. Wang J, Denny J, Tian C, Kim S, Mo Y, Kovacs F, Song Z, Nishimura K, Gan Z, Fu R, Quine JR, Cross TA. Imaging membrane protein helical wheels. J Magn Reson. 2000; 144:162–167. [PubMed: 10783287]

110. Wang S, Munro RA, Shi L, Kawamura I, Okitsu T, Wada A, Kim SY, Jung KH, Brown LS, Ladizhansky V. Solid-state NMR spectroscopy structure determination of a lipid-embedded heptahelical membrane protein. Nature methods. 2013; 10:1007–1012. [PubMed: 24013819]

111. Waugh JS, Huber LM, Haeberlen U. Approach to high-resolution NMR in solids. Physical Review Letters. 1968; 20:180–182.

112. Waugh JS. Uncoupling of local field spectra in nuclear magnetic resonance: Determination of atomic position in solids. Proc Natl Acad Sci U S A. 1976; 73:1394–1397. [PubMed: 1064013]

113. Weingarth M, Baldus M. Solid-State NMR-Based Approaches for Supramolecular Structure Elucidation. Accounts of chemical research. 2013; 46:2037–2046. [PubMed: 23586937]

114. Wilson JR, Leang C, Morby AP, Hobman JL, Brown NL. MerF is a mercury transport protein: different structures but a common mechanism for mercuric ion transporters? FEBS Letters. 2000; 472:78–82. [PubMed: 10781809]

115. Wu B, Chien EY, Mol CD, Fenalti G, Liu W, Katritch V, Abagyan R, Brooun A, Wells P, Bi FC, Hamel DJ, Kuhn P, Handel TM, Cherezov V, Stevens RC. Structures of the CXCR4 chemokine GPCR with small-molecule and cyclic peptide antagonists. Science. 2010; 330:1066–1071. [PubMed: 20929726]

116. Wu CH, Ramamoorthy A, Opella SJ. High-resolution heteronuclear dipolar solid-state NMR spectroscopy. J Magn Reson A. 1994; 109:270–272.

117. Wylie BJ, Sperling LJ, Niewuwkoop AJ, Franks WT, Oldfield E, Rienstra CM. Ultrahigh resolution protein strutures using NMR chemical shift tensors. Proc Natl Acad Sci. 2011; 108:16974–16979. [PubMed: 21969532]

118. Yan S, Suiter CL, Hou G, Zhang H, Polenova T. Probing structure and dynamics of protein assemblies by magic angle spinning NMR spectroscopy. Accounts of chemical research. 2013 in press.

119. Zhou HX, Cross TA. Influences of membrane mimetic environments on membrane protein structures. Annu Rev Biophys. 2013; 42:361–392. [PubMed: 23451886]

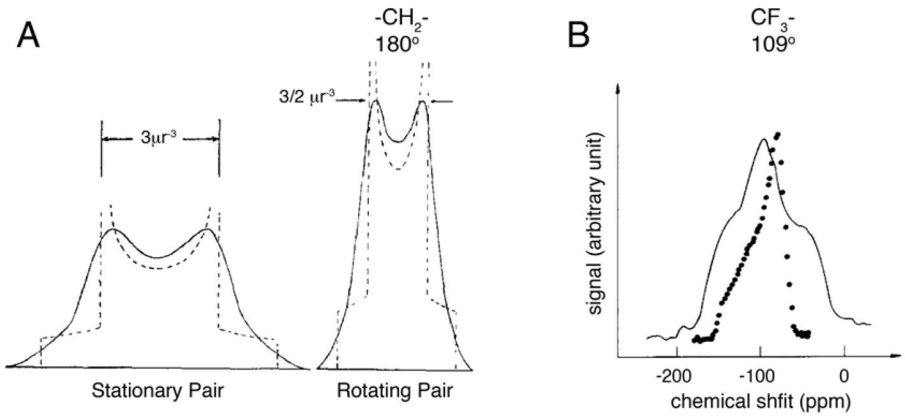

Figure 1.

The effects of rotational motion on dipole-dipole coupling and chemical shift anisotropy powder patterns. A. Theoretical line shapes for a nuclear pair with spin ½ when stationary and when in motion about an axis perpendicular to the internuclear axis. From reference [34]. B. ^{19}F powder spectra of silver trifluoroacetate at 107 K (.) and 40 K (−). The spectra are characteristic of rotating (107 K) and rigid (40 K) CF_3 groups. From reference [58].

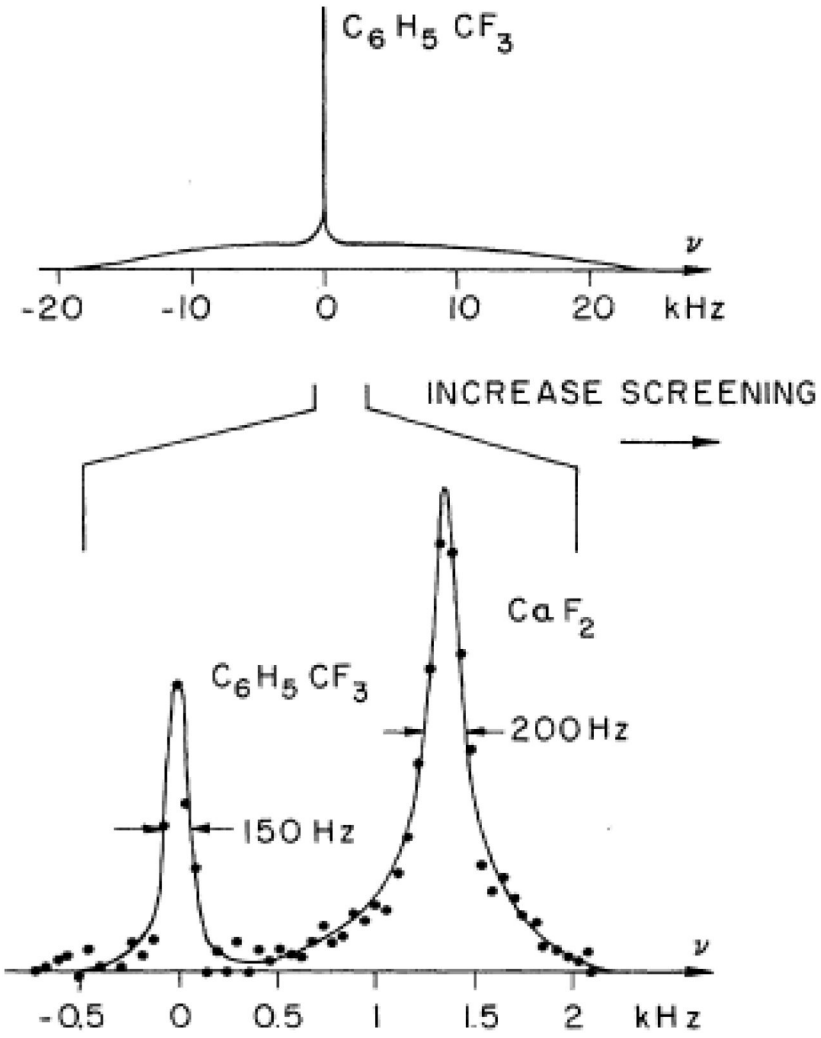

Figure 2.

^{19}F NMR spectra of a single crystal of CaF_2 wet with $C_6H_5CF_3$. Top spectrum: Fourier transform of a continuously sampled Bloch decay showing the sharp resonance of the liquid portion of the sample superimposed on the very broad resonance of the crystalline portion of the sample. Bottom spectrum: Fourier transform of the data points collected once per cycle in a delay between pulses in a four-pulse WaHuHa experiment showing the narrowing of the broad CaF_2 resonance and the preservation of the chemical shift difference between the two types of ^{19}F in the sample. From reference [111].

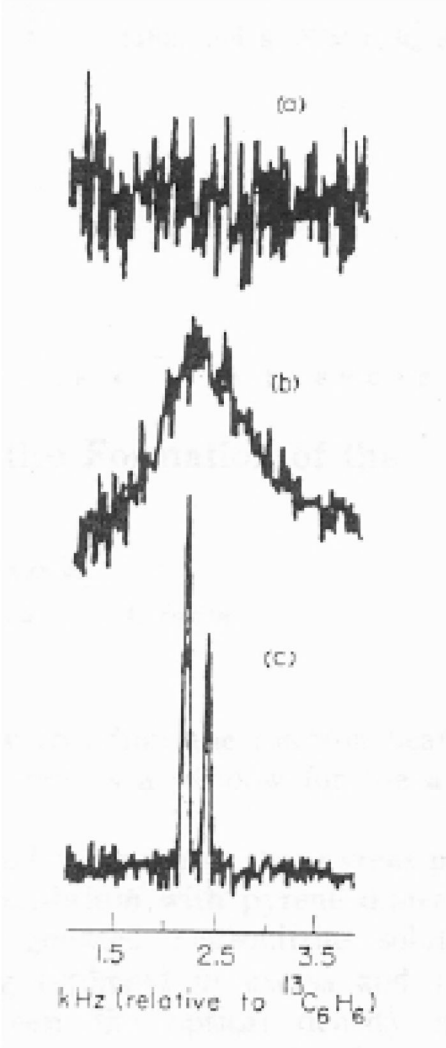

Figure 3.

Fourier transform NMR spectra of natural-abundance ^{13}C in polycrystalline adamantane at 24.46 MHz and room temperature. (a) Result of single free induction decay. (b) Cross-polarization spectrum without decoupling. (c) Cross-polarization spectrum with proton decoupling (14 contacts) obtained in 0.8 sec. From reference [86].

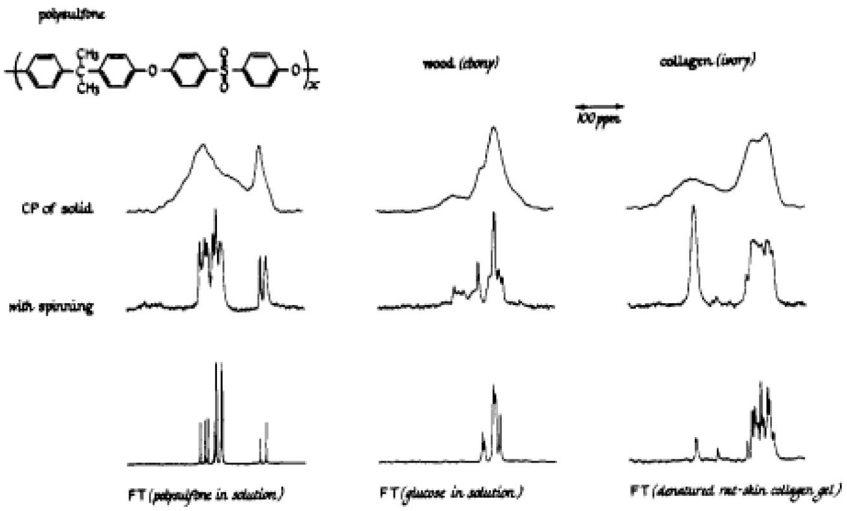

Figure 4.

Dipolar-decoupled natural abundance ^{13}C NMR spectra of some solids obtained using single Hartmann-Hahn cross-polarization contacts of 1 ms duration. The cross-polarization spectra, obtained both with and without magic-angle spinning, are compared to some standard Fourier transform ^{13}C NMR spectra of various materials in solution. Each spectrum is 8 kHz wide (at 22.6 MHz). The magnetic field increases from left to right. From reference [95].

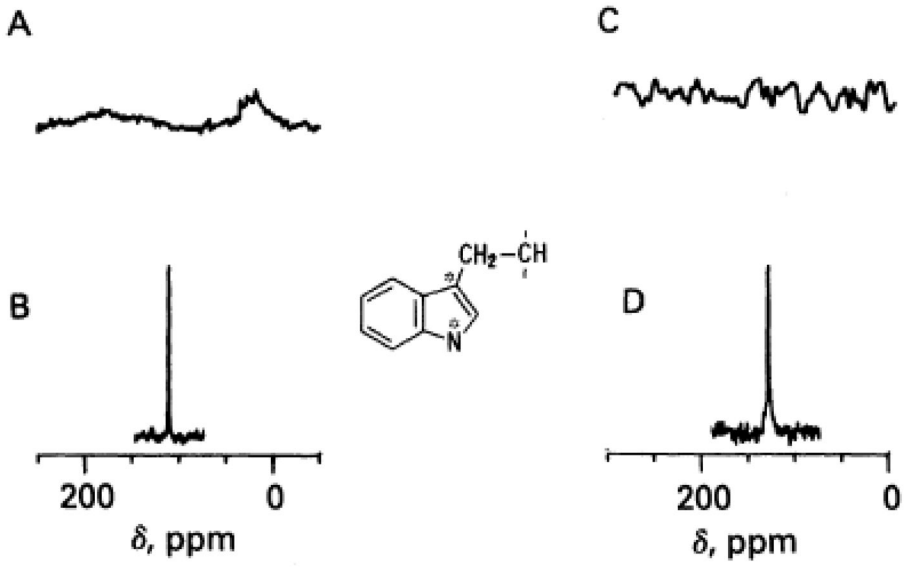

Figure 5.

^{13}C and ^{15}N NMR spectra of fd. A. Natural-abundance ^{13}C NMR spectrum of fd obtained with solution NMR methods. B. ^{13}C NMR spectrum of $^{13}C\gamma$-Trp-26-labeled fd obtained with cross-polarization, high-power proton decoupling, and rapid magic-angle sample spinning. C. Natural-abundance ^{15}N NMR spectrum of fd, similar to A. D. ^{15}N NMR spectrum of $^{15}N\varepsilon 2$-Trp-26-labeled fd, similar to B. Asterisks indicate the labeled atoms in the amino acid. From reference [31].

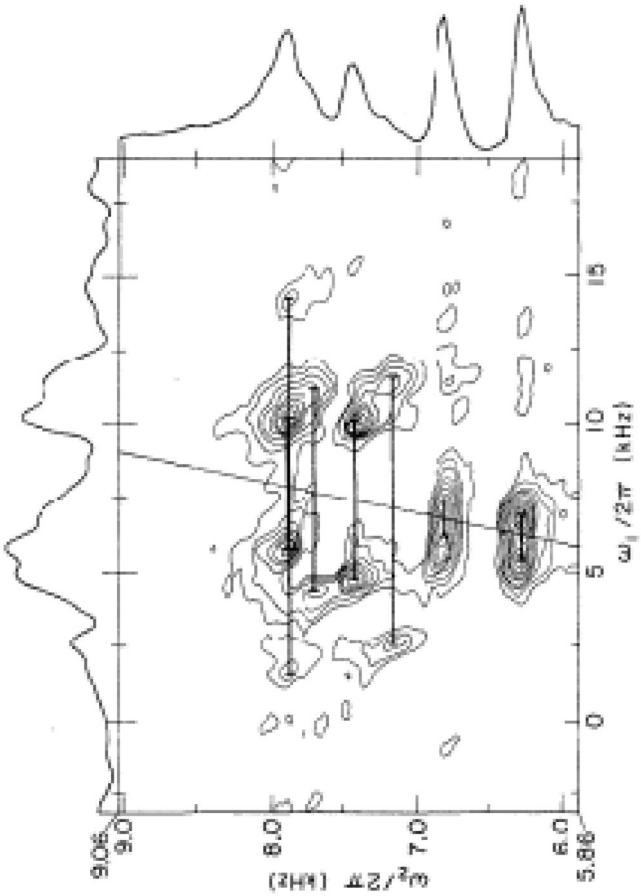

Figure 6.

Pure one-dimensional chemical shift spectrum (top) and two-dimensional SLF spectrum (bottom) for ^{13}C in a single crystal of calcium formate. A projection of the dipolar couplings is aligned on the left of the two-dimensional SLF spectrum. From reference [38].

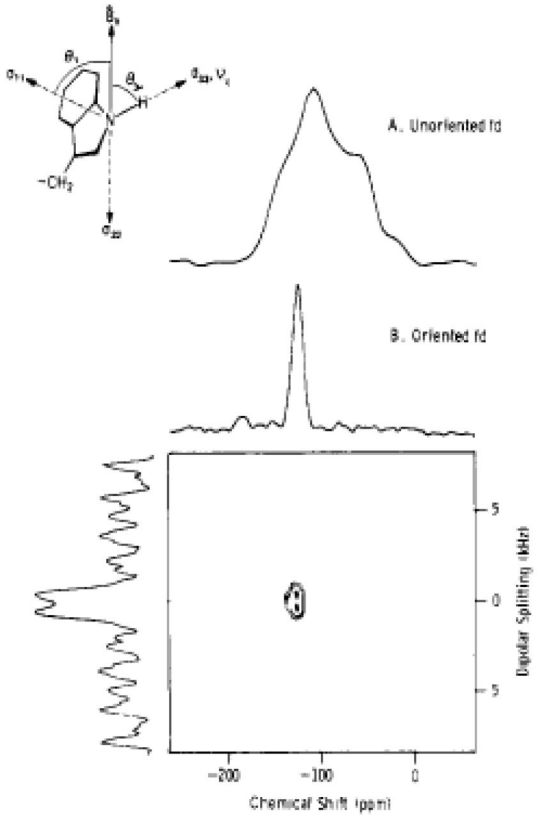

Figure 7.

^{15}N NMR spectra of ^{15}Nε2-Trp-26-labeled fd in solution. A. Chemical shift powder pattern for an unoriented sample; B. Chemical shift spectrum of an oriented sample. The contour plot represents the data from a two-dimensional separated local field experiment using off-resonance ^{1}H irradiation to suppress ^{1}H-^{1}H interactions; the projection of the dipolar splitting is aligned on the left side. The spin-interaction tensors are drawn schematically in the molecular frame of the tryptophan side chain. From reference [25].

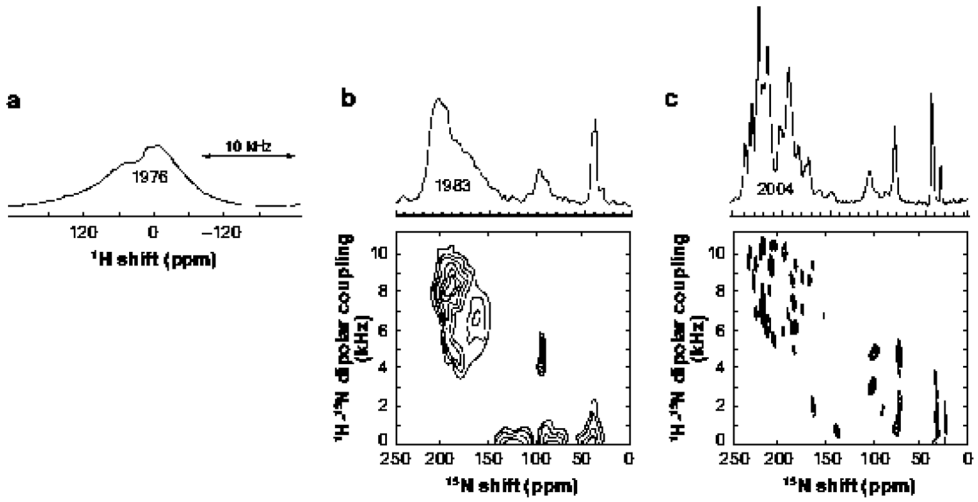

Figure 8.

Filamentous bacteriophages have served as an important test bed for the development of nuclear magnet resonance methods. a. A conventional solution-state NMR spectrum, obtained in 1976, showing low resolution and intensity. Spectra obtained in b. 1983 and c. 2004 on essentially identical samples of uniformly ^{15}N-labeled Pf1 bacteriophage. The two-dimensional separated local field spectra of magnetically aligned samples illustrate the improvements in instrumentation and experimental methods. From reference [71].

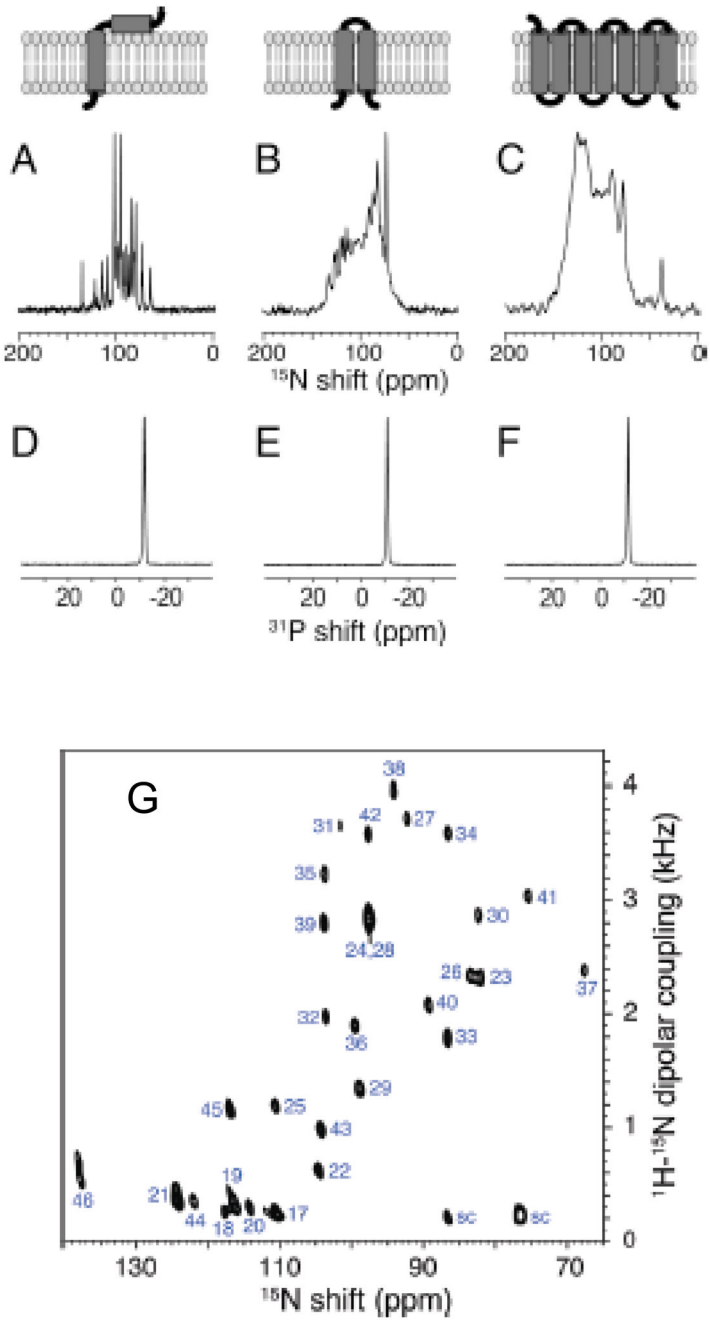

Figure 9.

(top) Schematic drawings of three membrane proteins aligned in planar "long-chain lipid": Triton X-100 (q=5) bilayers. A.-C. One-dimensional solid-state ^{15}N NMR spectra of uniformly ^{15}N-labeled proteins. D.–F. One-dimensional solid-state ^{31}P NMR spectra of the phospholipids in the same samples. A, D. The membrane-bound form of the 46-residue Pf1 coat protein. B, E. The 78-residue mercury transport protein MerE. C, F. The 350-residue G-protein-coupled receptor CXCR1. G. Two-dimensional SLF spectrum of uniformly ^{15}N-labeled Pf1 coat protein in DMPC:Triton X-100 bilayers obtained at 700 MHz with the SAMPI4 pulse sequence. From reference [80].

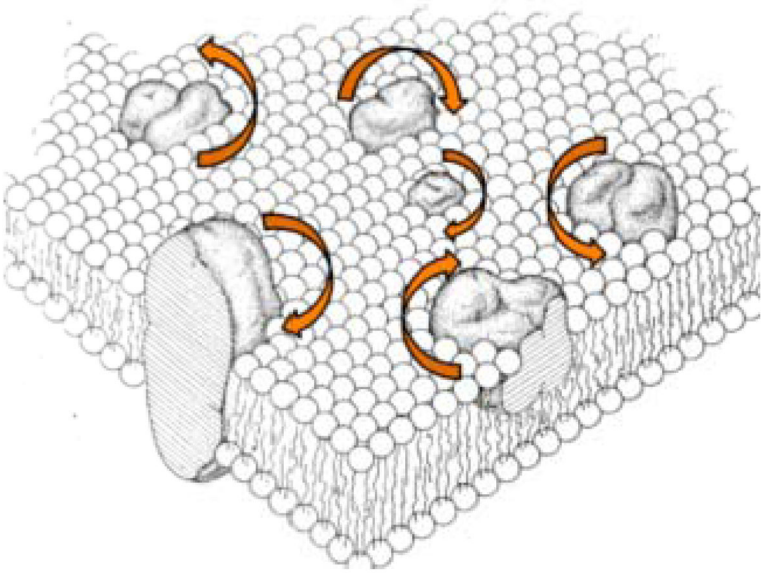

Figure 10.
Schematic three-dimensional and cross-sectional views of the “Fluid mosaic model” of globular membrane proteins that are completely or partially embedded within a lipid matrix. Modified from Singer and Nicholson [101]. From reference [72].

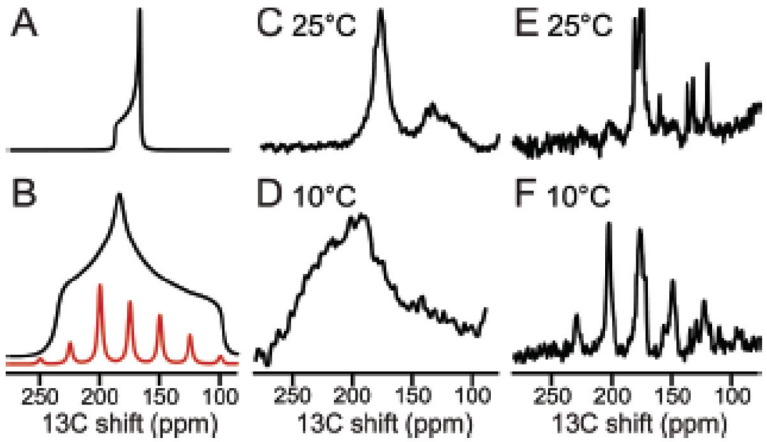

Figure 11.

^{13}C solid-state NMR spectra of uniformly $^{13}C/^{15}N$ labeled MerFt in DMPC proteoliposomes. The majority of resonance intensity centered near 175 ppm is from $^{13}C'$ backbone sites. A. Spectrum simulated for a single $^{13}C'$ group in a transmembrane helix undergoing rotational diffusion around the lipid bilayer normal. B. As in Panel A except for a static $^{13}C'$ group in a peptide bond. The family of sidebands in panel B (red) would be observed under slow (5 kHz) MAS. C. and D. Experimental spectra obtained for a stationary sample when the protein undergoes fast rotational diffusion about the phospholipid bilayer normal C. or where the protein is immobile on the time scale of the static $^{13}C'$ CSA powder pattern D. E. and F. Experimental spectra obtained from a sample undergoing slow (5 kHz) MAS where the $^{13}C'$ CSA powder pattern is motionally averaged E, or at where a family of sidebands spanning the width of the static $^{13}C'$ CSA powder pattern F is observed in the absence of protein rotational diffusion. Comparisons of the powder pattern frequency breadth (A vs. B; C vs. D) or the presence of spinning sidebands (E vs. F) are diagnostic for the presence of fast rotational diffusion of the protein under the experimental conditions used to measure the CSA and DC powder patterns. From reference [28].

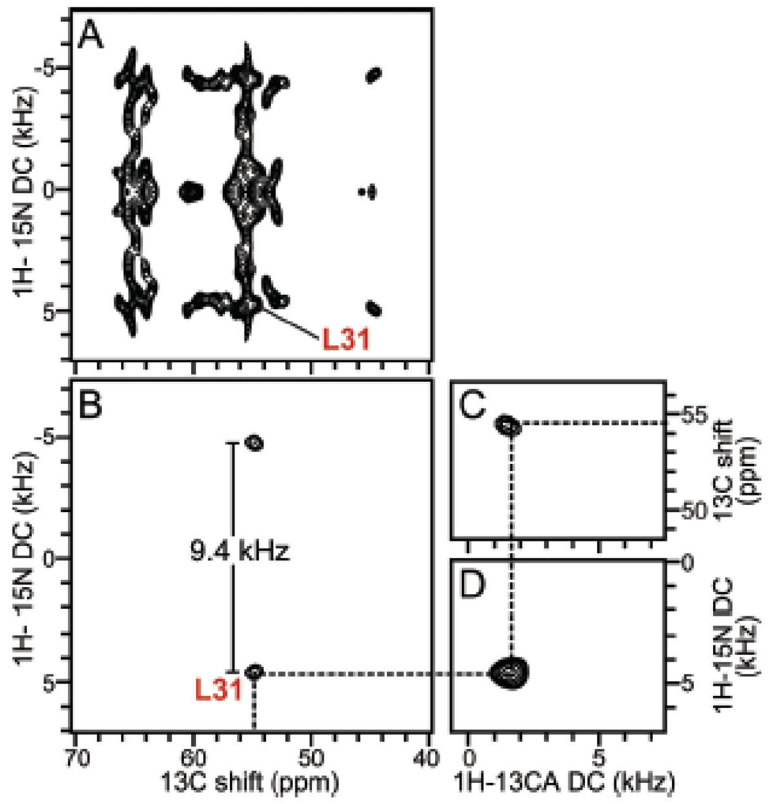

Figure 12.

Examples of spectroscopic data for residue L31 obtained from MAS solid-state NMR spectra of uniformly $^{13}C/^{15}N$ labeled MerFt in DMPC proteoliposomes at 25°C: A. two-dimensional ^{1}H-^{15}N dipolar coupling/^{13}C shift SLF spectrum, B. two-dimensional ^{1}H-^{15}N dipolar coupling/^{13}C shift SLF spectral plane selected from a three-dimensional spectrum at an isotropic ^{15}N chemical shift frequency of 118.6 ppm. C. Two-dimensional ^{1}H-^{13}CA dipolar coupling/^{13}C shift SLF spectral plane selected from a three-dimensional spectrum at an isotropic ^{15}N chemical shift frequency of 118.6 ppm. D. Two-dimensional ^{1}H-^{13}CA dipolar coupling/^{1}H-^{15}N dipolar coupling SLF spectral plane selected from a three-dimensional spectrum at an isotropic ^{13}C chemical shift frequency of 54.6 ppm. All three spectral planes are associated with residue L31. The dashed line traces the correlations among the frequencies, which were obtained from three separate experiments. The dipolar coupling frequencies in the spectra correspond to the perpendicular edge frequencies of the corresponding powder patterns. Panel B shows that the ^{1}H-^{15}N dipolar coupling motionally averaged powder pattern for L31 has a perpendicular edge frequency of 4.7 kHz, corresponding to a splitting of 9.4 kHz, and a dipolar coupling value of 18.8 kHz. From reference [28].

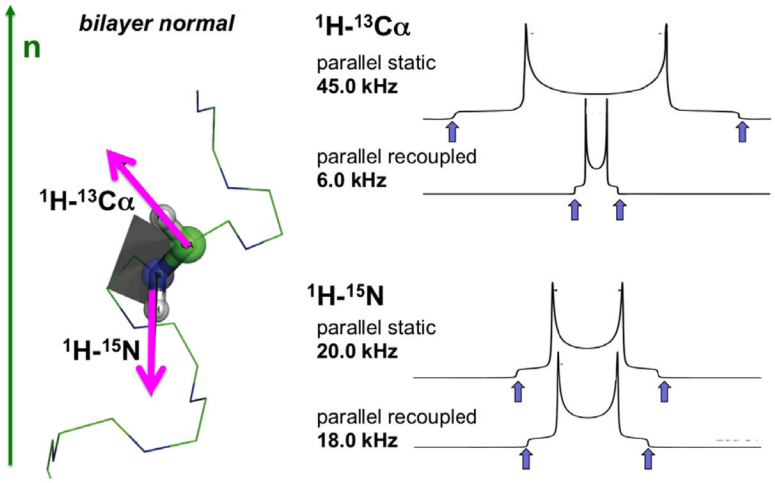

Figure 13.

Orientation of the peptide plane associated with residue L31 based on the experimental data shown in Figure 12.

A.) Initial calculation in Rosetta.

1. Input
   - Amino acid sequence.
   - Isotropic chemical shifts.
   - DC orientational restraints.
2. Generate fragment candidates in CS-Rosetta.
3. Calculate and refine structures with multiple rounds in Rosetta.
4. Extract dihedral angles from 1000 low-energy decoys.
5. Calculate average dihedrals for each residue from 1000 decoys.

B.) Refinement in XPLOR-NIH.

- Average dihedral angles from Rosetta structures.
- DC orientational restraints.
- CSA orientational restraints.
- Distance restraints.

C.) Evaluate structure.

- Calculate RMSD.
- Calculate R^2 for back calculated vs. experimental data.

Figure 14.

Outline of the protocol used to calculate the three-dimensional structures of proteins based on data such as that shown in Figure 12.

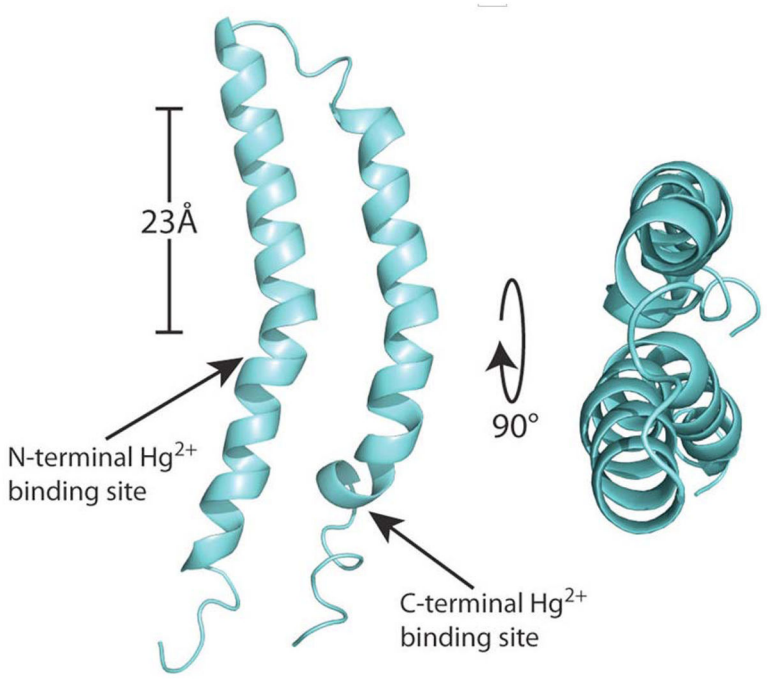

Figure 15.

The three-dimensional structure of MerF is shown as a ribbon diagram in aqua with the two mercury-binding sites labeled with arrows. The scale bar corresponds to the 23 Å thickness of the hydrocarbons in the lipid bilayer. Both termini of the protein are in the cytosol. From reference [52].

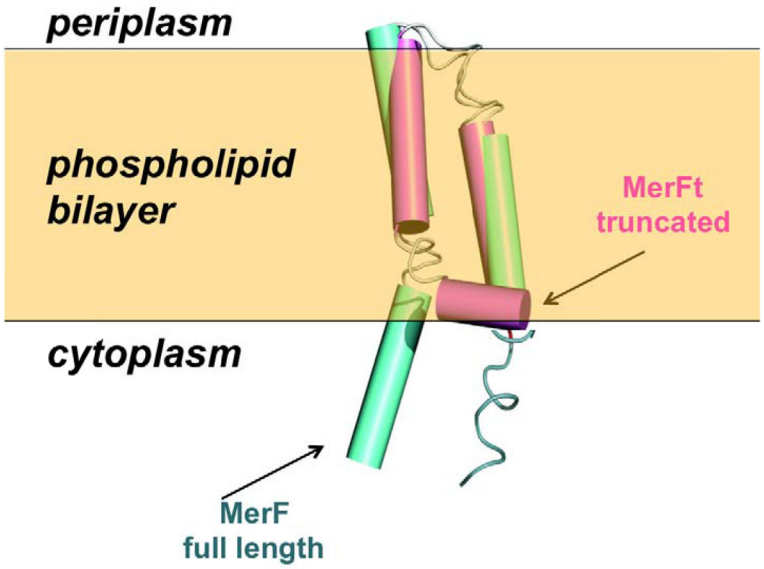

Figure 16.
The structure of the truncated 60-residue MerFt protein (magenta) is superimposed on the structure of the full-length 81-residue protein, MerF (aqua). From reference [52].

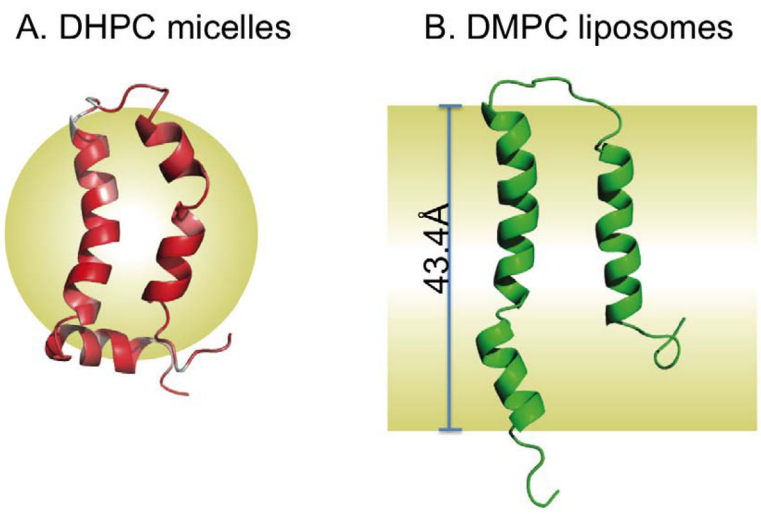

Figure 17.

Structures of the 63-residue full-length p7 protein. A. The structure determined in DHPC micelles by solution NMR (magenta) is shown in a micelle. B. The structure determined in DMPC bilayers by solid-state NMR (aqua) is shown in a bilayer. The solution NMR structure is from reference [22].

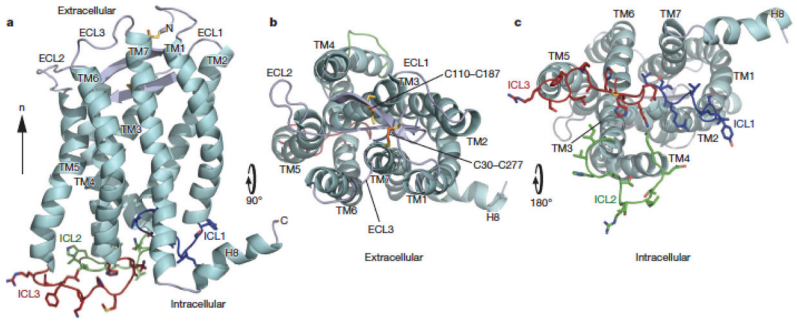

Figure 18.

Three-dimensional structure of CXCR1. Backbone representation of CXCR1 showing helices in cyan (TM1-TM7 and H8), extracellular loops in grey (ECL1-ECL3), and intracellular loops in blue (ICL1), green (ICL2) and red (ICL3). Disulfide-bonded Cys pairs (Cys30-Cys 277 and Cys110-Cys 87) are shown as sticks. a. Side view (n denotes bilayer normal), b. View from the extracellular side. c. View from the intracellular side. From reference [82].